第 43 卷 第 24 期/2023 年 12 月/光学学报 研究论文

光学学报

海洋湍流中厄米-高斯光束的传输特性研究

杜星[1,2]，丁桂璇[1,2]，杜浩[1,3*]，王生[1,2]，冯慧[1,3]

[1]中国科学院空天信息创新研究院，北京 101408；

[2]中国科学院大学，北京 100049；

[3]海南空天信息研究院海南省地球观测重点实验室，海南 文昌 571300

摘要 研究了海洋湍流中部分相干厄米-高斯光束的传输特性。首先，根据广义惠更斯-菲涅耳原理，建立了海洋湍流中厄米-高斯光束的强度分析模型。然后，推导了海洋湍流中厄米-高斯光束的均方束腰宽、瑞利区间和湍流距离的表达式。最后，对海洋湍流中厄米-高斯光束的均方束腰宽、瑞利区间和湍流距离进行仿真分析。仿真结果表明，均方束腰宽随着均方温度耗散率和温度与盐度相对参数的增大而增加，随着湍流动能耗散率的增大而减小。此外，瑞利区间和湍流距离都随着厄米-高斯光束的阶数的增加而增大。该研究可以为水下光通信研究提供理论依据。

关键词 水下光通信；厄米-高斯光束；海洋湍流；传输特性

中图分类号 O436 **文献标志码** A **DOI**：10.3788/AOS230644

1 引 言

近年来，水下通信技术逐渐成为水下探测和资源开发的关键技术之一[1-4]。在实际应用中，水下平台之间的通信基本采用超低频/甚低频（SLF/VLF）[5]。相比于SLF/VLF存在的传输带宽窄、安全性不足等问题，水下激光通信可以提供更大的传输带宽和更小的传输延迟[6]。因此，水下激光通信技术已成为研究热点之一。

在实际的光通信应用中，高斯光束常被用作激光通信信号的载体。但高斯光束在海水中传输时其强度会受到海洋湍流的削弱，并产生光斑漂移、光束拓展和光强起伏，这成为了制约水下激光通信距离的原因之一[7]。近年来，研究者们对高斯光束在湍流介质中的传播进行了大量的研究[8-23]。Yi等[8]对孔径平均闪烁指数、平均信噪比和平均误码率进行了分析。陈斐楠等[9]研究了部分相干厄米高斯光束在海洋湍流中光束传输质量的变化。赵英俊等[10]分析了海上厄米-高斯光束激光大气传输特性。Shchepakina等[11-13]研究了湍流海洋中高斯光束的强度、轨道角动量和有效曲率半径。Tang等[14]研究了海洋湍流中高斯阵列光束有效传输区域。Lu等[15]推导出了海洋湍流中M×N高斯光束平均强度的表达式。Yousefi等[16]分析了海洋湍流中部分相干平顶激光束的平均强度分布。Mao等[17]推导出了海洋湍流中多径向高斯-谢尔模型阵列光束的平均强度的解析公式。但是，这些研究仍然以高斯光束为主要对象。

值得注意的是，作为降低湍流影响的有效方法之一，使用厄米-高斯光束进行激光传输已经在大气湍流中被证实具有更大的瑞利区间和湍流距离[18]。其中，陈晓文等[19]推导了部分相干厄米-高斯光束在大气湍流中传输的湍流距离表达式。汤明玥[20]研究了厄米-高斯光束在大气湍流中的远场光束质量。张笔灵等[21]研究了厄米-高斯谢尔光束在大气湍流的漂移。Yang等[22]研究了部分相干标准厄米-高斯束在大气湍流中的传播特性。Zhao等[23]研究了厄米-余弦高斯谢尔光束在非Kolmogorov大气湍流中的传播。然而，根据文献调研结果，关于海洋湍流中的厄米-高斯光束的均方束腰宽、瑞利区间和湍流距离的研究还未见报道。

本文建立了一个分析厄米-高斯光束通过海水传播的理论模型。基于广义惠更斯-菲涅耳原理，推导了光束均方束腰宽、瑞利区间和湍流距离的解析表达式。然后，研究了高斯光束的瑞利区间等参数与海洋湍流参数的关系并给出了合理的物理解释。该研究结果对水下光通信系统设计具有借鉴和指导意义。

2 厄米-高斯光束在海洋湍流中的理论模型

厄米-高斯光束在海洋湍流中的传输过程如图1所示，其中z是传输距离（从光源平面到接收平面）。

收稿日期：2023-03-07；**修回日期**：2023-04-11；**录用日期**：2023-04-24；**网络首发日期**：2023-05-08

基金项目：海南省自然科学基金（622MS105，620MS076）

通信作者：*duhao@aircas.ac.cn

光束在海水中传输时会受到海洋湍流的作用，产生光束拓展。因此，湍流会影响光束的均方宽度，进一步改变光束的瑞利区间和湍流距离。本节主要推导海洋湍流中厄米-高斯光束的均方束腰宽、瑞利区间和湍流距离的解析式，为后续的仿真研究提供理论基础。

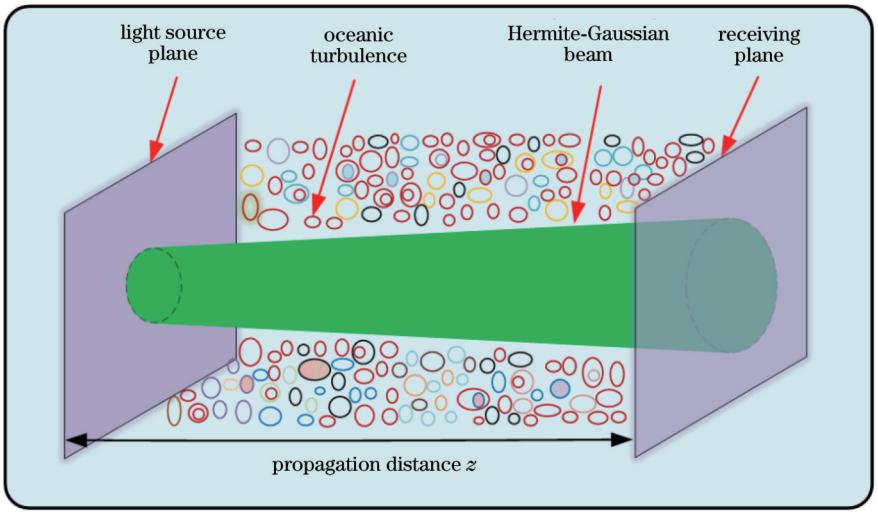

图 1　海洋湍流中的厄米-高斯光束传输示意图

Fig. 1　Schematic diagram of Hermite-Gaussian beam transmitting in the oceanic turbulence

2.1　厄米-高斯光束的光强

为了计算厄米-高斯光束的光强，首先建立海洋湍流中厄米-高斯光束的交叉谱密度函数模型。在海洋湍流中，$z=0$ 处的厄米-高斯光束（考虑一维情形）的交叉谱密度函数[11]可以写成

$$W^{(0)}(x_1', x_2', 0) = B_m^2 \exp\left[-\frac{x_1'^2 + x_2'^2}{w_0^2}\right] \times \exp\left[-\frac{(x_1' - x_2')^2}{2\sigma_0^2}\right] H_m\left[\frac{\sqrt{2}\, x_1'}{w_0}\right] H_m\left[\frac{\sqrt{2}\, x_2'}{w_0}\right], \tag{1}$$

式中：w_0 和 σ_0 分别为 $z=0$ 处的厄米-高斯光束的腰宽和相干长度；H_m 代表 m 阶厄米多项式；$B_m^2 = \sqrt{2}/(\sqrt{\pi}\, 2^m w_0 m!)$。

然后，根据广义惠更斯-菲涅耳原理，部分相干厄米-高斯光束在海洋湍流中传输的交叉谱密度函数[11]可表示为

$$W(x_1, x_2, z) = \frac{k}{2\pi z} \iint \mathrm{d}x_1' \mathrm{d}x_2' W^0(x_1', x_2', 0) \times \exp\left\{-\frac{\mathrm{i}k}{2z}\left[(x_1 - x_1')^2 - (x_2 - x_2')^2\right]\right\} \times \left\langle \exp\left[\psi^*(x, x_1', z) + \psi(x, x_2', z)\right]\right\rangle_m 。 \tag{2}$$

在海洋湍流中，部分相干厄米-高斯光束的光强可以表示为

$$I(x, z) = W(x, x, z) = \frac{k}{2\pi z} \iint W^{(0)}(x_1', x_2', 0) \exp\left[-\mathrm{i}k \frac{(x - x_1')^2 - (x - x_2')^2}{2z}\right] \times \left\langle \exp\left[\psi^*(x, x_1', z) + \psi(x, x_2', z)\right]\right\rangle_m \mathrm{d}x_1' \mathrm{d}x_2', \tag{3}$$

式中：$k=2\pi/\lambda$ 为波数，λ 是波长。$\langle\cdots\rangle_m$ 表示海洋湍流介质的系综平均值[11]，可以表示为

$$\exp\left[\psi^*(x, x_1', z) + \psi(x, x_2', z)\right]_m = \exp\left[-\frac{\pi^2 k^2 z (x_1' - x_2')^2}{3} \int_0^\infty \kappa^3 \Phi(\kappa) \mathrm{d}\kappa\right], \tag{4}$$

式中：$\Phi(\kappa)$ 为海洋湍流介质中折射率波动的空间功率谱。本文考虑各向同性均匀海洋湍流，并使用 Nikishov 模型描述，$\Phi(\kappa)$[11]可以表示为

$$\Phi(\kappa) = 0.388 \times 10^{-8} \varepsilon^{-1/3} \kappa^{-11/3} \left[1 + 2.35(\kappa\eta)^{2/3}\right] \frac{\chi_T}{w^2} \left[w^2 \exp(-A_T \delta) + \exp(-A_S \delta) - 2w \exp(-A_{TS} \delta)\right], \tag{5}$$

式中：ε 为湍流动能耗散率，取值范围为 $10^{-4} \sim 10^{-10}\ \mathrm{m^2 \cdot s^{-3}}$；$\eta$ 为 Kolmogorov 微尺度，取值为 $\eta = 10^{-3}$ m，χ_T 为均方温度耗散率，从海洋表面到深水层的取值范围是 $10^{-2} \sim 10^{-10}\ \mathrm{k^2 \cdot s^{-1}}$；$w$ 为与温度和盐度相关的参数，其取值范围是 $-5 \sim 0$，$w=-5$ 代表湍流以温度诱致为主，$w=0$ 代表湍流以盐度诱致为主；$A_T = 1.863 \times 10^{-2}$，$A_S = 1.9 \times 10^{-4}$，

$A_{TS}=9.41\times10^{-3}$, $\delta=8.284(\kappa\eta)^{4/3}+12.978(\kappa\eta)^{2}$。

2.2 均方束腰宽

为了对式(3)进行积分运算,引入变量$s=(x_1'+x_2')/2$, $t=x_2'-x_1'$, 则部分相干厄米-高斯光束通过海洋湍流传输的平均光强可表示为

$$I(x,z)=\frac{k}{2\pi z}B_m^2\iint \mathrm{d}s\mathrm{d}t H_m\left[\frac{\sqrt{2}}{w_0}\left(s+\frac{1}{2}t\right)\right]\times H_m\left[\frac{\sqrt{2}}{w_0}\left(s-\frac{1}{2}t\right)\right]\exp\left(-\frac{2s^2}{w_0^2}\right)\exp\left(-\frac{t^2}{2w_0^2}\right)\times$$
$$\exp\left(-\frac{t^2}{2\sigma_0^2}\right)\times\exp\left(-\mathrm{i}\frac{k}{z}st\right)\times\exp\left(\mathrm{i}\frac{k}{z}xt\right)\times\exp\left[-\frac{\pi^2k^2t^2z}{3}\int_0^\infty\kappa^3\Phi(\kappa)\mathrm{d}\kappa\right]。\tag{6}$$

根据海洋湍流中均方束腰宽[14]的定义,即

$$\langle x^2\rangle_{\mathrm{turb}}=\frac{4\int x^2\langle I(x,z)\rangle\mathrm{d}x}{\int\langle I(x,z)\rangle\mathrm{d}x}。\tag{7}$$

进一步,式(7)可以被改写成

$$\langle x^2\rangle_{\mathrm{turb}}=\frac{4I_{F1}}{I_{F2}},\tag{8}$$

其中

$$I_{F1}=\int x^2\langle I(x,z)\rangle\mathrm{d}x,\tag{9}$$
$$I_{F2}=\int\langle I(x,z)\rangle\mathrm{d}x。\tag{10}$$

这里,引入积分公式来进行直接的积分运算

$$\int x^2\exp(-\mathrm{i}2\pi xs)\mathrm{d}x=-\frac{1}{(2\pi)^2}\delta''(s),\tag{11}$$

$$\int\exp(-x^2)H_m(x+y)H_m(x+z)\mathrm{d}x=$$
$$2^m\sqrt{\pi}\,L_m(-2yz),\tag{12}$$
$$\int f(x)\delta''(x)\mathrm{d}x=f''(0)。\tag{13}$$

把式(6)代入式(9),并且利用式(11)、(12),可以得出

$$I_{F1}=-\left(\frac{z}{k}\right)^2\frac{1}{m!}\int\exp(\Im_At^2)L_m(\Im_Bt^2)\delta''(t)\mathrm{d}t,\tag{14}$$

其中

$$\Im_A=-\left[\frac{1}{2w_0^2}+\frac{1}{2\sigma_0^2}+\frac{k^2w_0^2}{8z^2}+\frac{\pi^2k^2z}{3}\int_0^\infty\kappa^3\Phi(\kappa)\mathrm{d}\kappa\right],\tag{15}$$

$$\Im_B=\frac{1}{w_0^2}+\frac{k^2w_0^2}{4z^2}。\tag{16}$$

然后,根据式(13)可以得到

$$I_{F1}=-\left(\frac{z}{k}\right)^2\frac{1}{m!}\left.\frac{\mathrm{d}\left[\exp(\Im_At^2)L_m(\Im_Bt^2)\right]}{\mathrm{d}t}\right|_{t=0}。\tag{17}$$

计算微分,然后得出

$$I_{F1}=\frac{(1+2m)w_0^2}{4}+\frac{1}{k^2w_0^2}\left(1+2m+\frac{w_0^2}{\sigma_0^2}\right)z^2+$$
$$\frac{2}{3}\pi^2\left[\int_0^\infty\kappa^3\Phi(\kappa)\mathrm{d}\kappa\right]z^3。\tag{18}$$

类似地,可以得到

$$I_{F2}=\int\langle I(x,z)\rangle\mathrm{d}x=1。\tag{19}$$

把式(18)、(19)代入式(8)并整理,可以得到光束均方束腰宽的表达式,即

$$\langle x^2\rangle_{\mathrm{turb}}=\Theta_A+\Theta_Bz^2+\wp_Tz^3,\tag{20}$$

其中

$$\Theta_A=(1+2m)w_0^2,\ \Theta_B=\frac{4}{k^2w_0^2}\left(1+2m+\frac{1}{\ell_k^2}\right),\ \ell_k=$$
$$\sigma_0/w_0,\ \wp_T=\frac{8}{3}\pi^2\int_0^\infty\kappa^3\Phi(\kappa)\mathrm{d}\kappa。\tag{21}$$

2.3 瑞利区间和湍流距离

1) 瑞利区间

瑞利区间z_R表征光束的准直区间,定义为光束的横截面积达到场源处两倍时的传播距离[24], z_R可以表示为

$$\langle x^2\rangle_{\mathrm{turb}}\Big|_{z=z_R}=2\langle x^2\rangle_{\mathrm{turb}}\Big|_{z=0},\tag{22}$$

把式(20)代入到式(22)中,可以得到

$$z_R=\frac{1}{3\wp_T}\left(\Xi+\frac{\Theta_B^2}{\Xi}-\Theta_B\right),\tag{23}$$

其中

$$\Xi=\left[\frac{27}{2}\Theta_A\wp_T^2-\Theta_B^3+\frac{3}{2}\wp_T\left(81\Theta_A^2\wp_T^2-12\Theta_A\Theta_B^3\right)^{1/2}\right]^{1/3}。\tag{24}$$

2) 湍流距离

光束扩展受到湍流的影响可以由湍流距离z_T和z_{TT}描述,分别定义为光束横截面积扩展达10%和90%时的光束传输距离[25],即

$$\frac{\langle x^2(z_T)\rangle_{\mathrm{turb}}-\langle x^2(z_T)\rangle_{\mathrm{free}}}{\langle x^2(z_T)\rangle_{\mathrm{turb}}}=\eta_1,\ 0<\eta_1\leqslant0.1,\tag{25}$$

$$\frac{\langle x^2(z_{TT})\rangle_{\mathrm{turb}}-\langle x^2(z_{TT})\rangle_{\mathrm{free}}}{\langle x^2(z_{TT})\rangle_{\mathrm{turb}}}=\eta_2,\ 0.9\leqslant\eta_2<1,\tag{26}$$

式中:$\langle x^2(z_T)\rangle_{\mathrm{free}}$和$\langle x^2(z_{TT})\rangle_{\mathrm{free}}$分别表示自由空间中$z=z_T$和$z=z_{TT}$平面上的光束均方束腰宽;$\eta_1=0.1$;$\eta_2=0.9$。当$z<z_T$时湍流对激光束的影响很小,可以忽略不计,当$z>z_{TT}$时,激光束的扩散主要由湍流导致[22]。求解式(25)、(26)可以得到

$$z_T=\frac{R+\eta_1^2\Theta_B^2/R+\eta_1\Theta_B}{3(1-\eta_1)\wp_T},\tag{27}$$

$$z_{TT}=\frac{G+\eta_2^2\Theta_B^2/G+\eta_2\Theta_B}{3(1-\eta_2)\wp_T},\tag{28}$$

其中

$$R=\left\{\frac{27}{2}\eta_1\left(1-\eta_1\right)^2\Theta_A\wp_{\mathrm{T}}^2+\eta_1^3\Theta_B^3+\frac{3}{2}\left(1-\eta_1\right)\wp_{\mathrm{T}}\left[81\eta_1^2\left(1-\eta_1^2\right)\Theta_A^2\Theta_B^2+12\eta_1^4\Theta_A\Theta_B^3\right]^{1/2}\right\}^{1/3},\tag{29}$$

$$G=\left\{\frac{27}{2}\eta_2\left(1-\eta_2\right)^2\Theta_A\wp_{\mathrm{T}}^2+\eta_2^3\Theta_B^3+\frac{3}{2}\left(1-\eta_2\right)\wp_{\mathrm{T}}\left[81\eta_2^2\left(1-\eta_2^2\right)\Theta_A^2\Theta_B^2+12\eta_2^4\Theta_A\Theta_B^3\right]^{1/2}\right\}^{1/3}。\tag{30}$$

3　数值仿真

基于上一节推导的理论公式，对海洋湍流中厄米-高斯光束的均方束腰宽、瑞利区间和湍流距离进行数值模拟。除非图中或图注中具体说明，仿真参数主要采用以下数值λ=0.532 μm，w_0=5 mm，η=1 mm，ε=10^{-4} m^2/s^3，w=−1，χ_{T}=10^{-10} K^2/s，仿真结果如下。

3.1　均方光束宽度

海洋湍流参数（均方温度耗散率χ_{T}、湍流动能耗散率ε、温度诱致和盐度诱致相关参数w）对海洋湍流中厄米-高斯光束的均方束腰宽的影响由图2（a）～（d）给出。从图中可以发现，均方束腰宽（图中省略尖括号和下标）随着均方温度耗散率的增大而增加，越接近海平面均方温度耗散率越大，说明光束在靠近海平面的区域宽度增长更快，在海水深处宽度增长较慢。其次，均方束腰宽随着湍流动能耗散率的增大而减小，并且在参数w取较小值时减小的程度更大。最后，更大的参数w决定了更大的光束均方束腰宽，因此盐度诱致占主导时光束均方束腰宽更大。

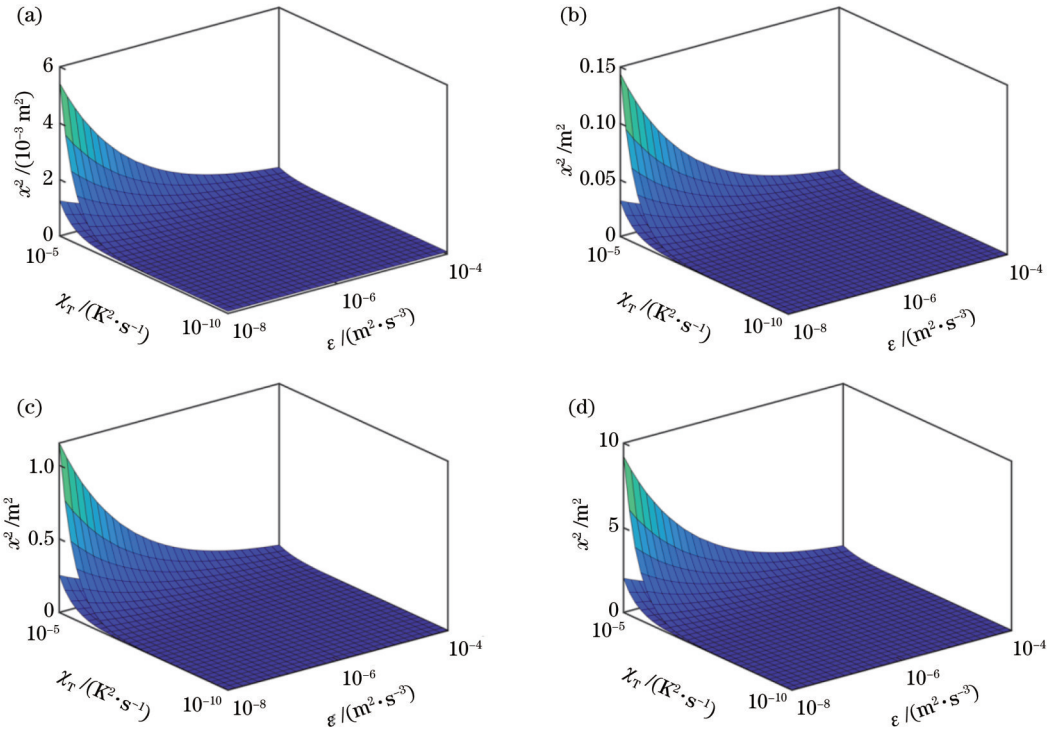

图2　均方光束宽度与海洋湍流参数χ_{T}、ε、w以及传输距离的关系（上下曲面分别对应w=−1，−3.5）。（a）z=25 m；（b）z=75 m；（c）z=150 m；（d）z=300 m

Fig. 2　Relationship between the mean square beam width and the ocean turbulence parameters χ_{T}, ε, w, and the transmission distance (w=−1, −3.5 correspond to the upper and lower surfaces, respectively). (a) z=25 m; (b) z=75 m; (c) z=150 m; (d) z=300 m

另一方面，图3展示了厄米-高斯光束在海洋湍流中传输时，不同的波长、相干长度和阶数对均方束腰宽的影响[分别对应于图3（a）～（c）]。从图3（a）可以发现，当波长的取值变化时，光束的均方束腰宽始终随着传输距离z的增大而增大。并且，在同样的传输距离时，更大的波长对应更大的均方束腰宽。然后研究了图3（b）中的曲线，可以发现相干长度（相对于波长）对光束均方束腰宽的影响更小，当传输距离一定时，相干长度越大光束的均方束腰宽越小。最后，研究了阶数（分别取阶数m=0，1，5）对均方束腰宽的作用[图3（c）]。从图中可以发现，阶数越大光束的均方束腰宽越大，并且阶数更大时均方束腰宽随距离增加而增大的趋势更明显。

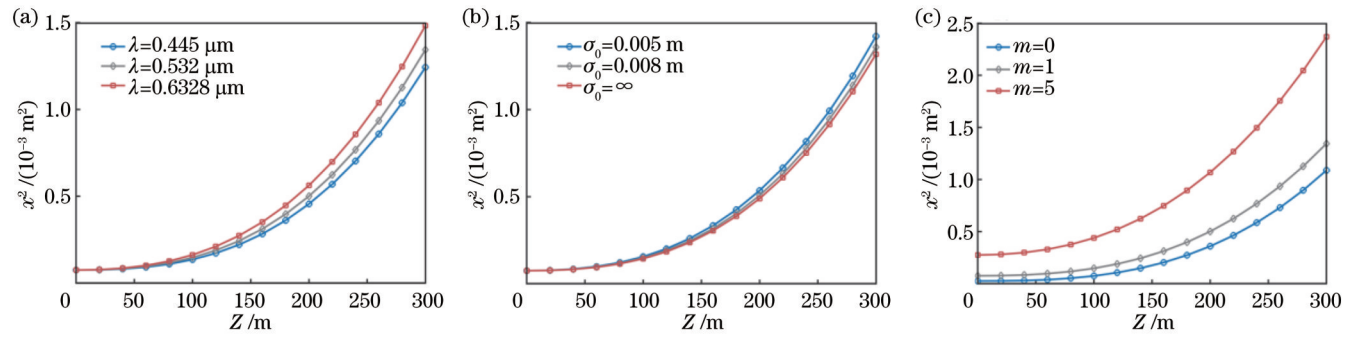

图 3　不同参数值时均方束腰宽与距离 z 的变化关系。(a) 不同波长下的均方束腰宽；(b) 不同相干长度下的均方束腰宽；(c) 不同阶数时的均方束腰宽

Fig. 3　Relationship between mean square beam width and distance z for different parameter values. (a) Mean square beam width for different wavelengths; (b) mean square beam width for different coherence lengths; (c) mean square beam width for different orders

3.2　瑞利区间

在 3.1 节研究光束均方束腰宽的基础上，进一步研究不同阶数厄米-高斯光束的瑞利区间受海洋湍流的影响（图 4）。从图 4 可以看出，瑞利区间 z_R 随着均方温度耗散率 χ_T、温度与盐度的相关参数 w 的增加而减小，随着湍流动能耗散率 ε 的增大而增大。值得注意的是，参数 w 和温度诱致与盐度诱致的相对强度有关。这意味着当盐度诱致占主导时，湍流作用更强，光束在其中扩展越快。并且，厄米-高斯光束的阶数越大，光束的瑞利区间越大，即光束扩展越慢，受湍流的影响越弱。

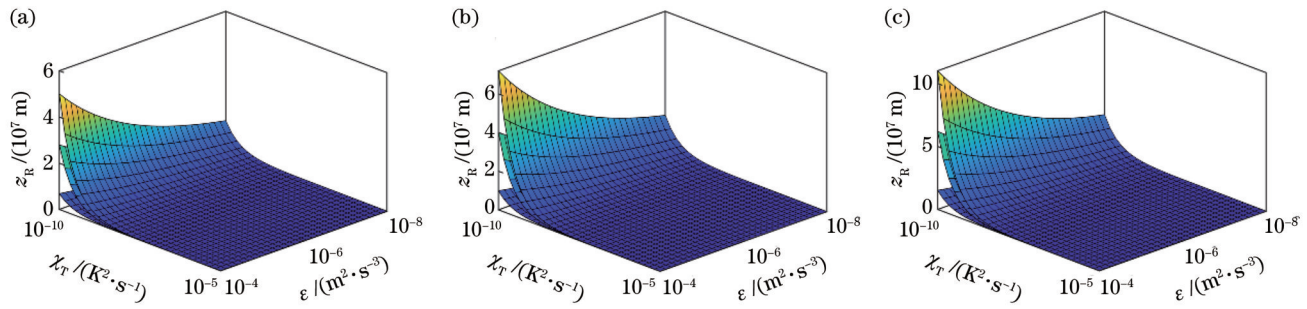

图 4　不同阶数厄米-高斯光束的瑞利区间随海洋湍流的变化（图中 $w=-0.1$，-1，-4.9，从下到上）。(a) $m=0$；(b) $m=1$；(c) $m=5$

Fig. 4　Rayleigh range of Hermite-Gaussian beam of different orders versus the oceanic turbulence parameters ($w=-0.1$, -1, and -4.9, from bottom to top). (a) $m=0$; (b) $m=1$; (c) $m=5$

3.3　湍流距离

图 5 为厄米-高斯阵列光束通过海洋湍流的湍流距离随海洋湍流参数的变化情况。从图 5(a) 可以看出，湍流距离随着均方温度耗散率 χ_T 的增大而减小。图 5(b) 展示了湍流距离随着参数 w 的增大而减小。在图 5(c) 中 z_T、z_{TT} 随着湍流动能耗散率 ε 的增大而增

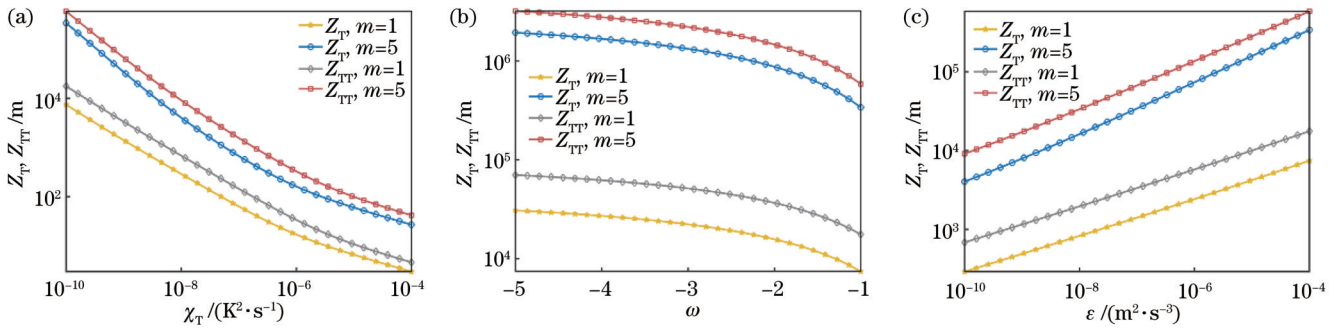

图 5　湍流距离 z_T、z_{TT} 与三个海洋湍流参数（χ_T，ε，w）的变化关系。(a) 均方温度耗散率；(b) 温度和盐度相对参数；(c) 湍流动能耗散率

Fig. 5　Changes between the turbulence distance of z_T, z_{TT} and the three ocean turbulence parameters (χ_T, ε, w). (a) Rate of dissipation of mean-square temperature; (b) relative strength of temperature and salinity; (c) turbulent dissipation

大。对于不同阶数的光束而言，阶数越高湍流距离越大，光束受湍流的干扰越小。

4 结 论

本文研究了部分相干厄米-高斯光束在海洋湍流中的传输特性。首先，根据广义惠更斯-菲涅耳原理推导出了厄米-高斯光束的交叉谱密度函数表达式，然后得出了厄米-高斯光束的均方束腰宽、瑞利区间和湍流距离的解析表达式。最后，我们研究了海洋湍流参数（均方温度耗散率、湍流动能耗散率、温度和盐度相对参数）和光学参数（波长、相干长度和阶数）对厄米-高斯光束传输特性的影响。结果表明，均方束腰宽随着均方温度耗散率和温度与盐度相对参数的增大而增加，随着湍流动能耗散率的增大而减小。并且，更高阶的厄米-高斯光束具有更大的均方束腰宽，瑞利区间和湍流距离都随着阶数的增加而增大。这意味着高阶的厄米-高斯光束具有更好的抵抗湍流扰动的能力。由于更大的瑞利区间和湍流距离决定了更长的有效通信距离，因此本文的研究结论对水下激光通信研究具有重要的意义和价值。

参 考 文 献

[1] He S H, Wang N, Ho M, et al. Design of a new stress wave communication method for underwater communication[J]. IEEE Transactions on Industrial Electronics, 2021, 68(8): 7370-7379.

[2] 石佳, 黄爱萍, 陶林伟. 深度学习辅助水下光通信信道估计和信号检测[J]. 中国激光, 2022, 49(17): 1706004.
Shi J, Huang A P, Tao L W. Deep learning aided channel estimation and signal detection for underwater optical communication[J]. Chinese Journal of Lasers, 2022, 49(17): 1706004.

[3] 韦育, 于永河, 黑小兵, 等. 涡旋光束和光子计数在水下光通信中的应用[J]. 激光与光电子学进展, 2022, 59(13): 1301001.
Wei Y, Yu Y H, Hei X B, et al. Application of vortex beam and photon counting in underwater optical communication[J]. Laser & Optoelectronics Progress, 2022, 59(13): 1301001.

[4] 万超, 郝浩, 赵清源, 等. 单光子探测在无线光通信收发技术中的应用[J]. 激光与光电子学进展, 2022, 59(5): 0500001.
Wan C, Hao H, Zhao Q Y, et al. Application of single photon detection in wireless optical communication transceiver technology[J]. Laser & Optoelectronics Progress, 2022, 59(5): 0500001.

[5] 王琛, 崔勇, 宋晓, 等. 基于驻极体材料的机械天线式低频/甚低频通信磁场传播模型[J]. 物理学报, 2020, 69(15): 158401.
Wang C, Cui Y, Song X, et al. Magnetic field propagation model of low frequency/very low communication based on mechanical antenna of electret[J]. Acta Physica Sinica, 2020, 69(15): 158401.

[6] Xu J, Lin A B, Yu X Y, et al. Underwater laser communication using an OFDM-modulated 520-nm laser diode[J]. IEEE Photonics Technology Letters, 2016, 28(20): 2133-2136.

[7] 陆璐. 海洋湍流对激光束传输的影响[D]. 合肥: 中国科学技术大学, 2016.
Lu L. Influence of ocean turbulence on laser beam propagation [D]. Hefei: University of Science and Technology of China, 2016.

[8] Yi X, Li Z, Liu Z J. Underwater optical communication performance for laser beam propagation through weak oceanic turbulence[J]. Applied Optics, 2015, 54(6): 1273-1278.

[9] 陈斐楠, 陈延如, 赵琦, 等. 部分相干厄米高斯光束在海洋湍流中光束传输质量的变化[J]. 中国激光, 2013, 40(4): 0413002.
Chen F N, Chen Y R, Zhao Q, et al. Change of propagation quality factor of partially coherence Hermite-Gaussian beams traveling through oceanic turbulence[J]. Chinese Journal of Lasers, 2013, 40(4): 0413002.

[10] 赵英俊, 王江安, 梁善勇, 等. 海上厄米-高斯光束激光大气传输特性[J]. 光电技术应用, 2009, 24(4): 21-24.
Zhao Y J, Wang J A, Liang S Y, et al. Atmosphere transmission characteristic of Hermite-Gaussian beam laser at sea [J]. Electro-Optic Technology Application, 2009, 24(4): 21-24.

[11] Shchepakina E, Farwell N, Korotkova O. Spectral changes in stochastic light beams propagating in turbulent ocean[J]. Applied Physics B, 2011, 105(2): 415-420.

[12] Li Y, Xie Y Q, Li B L. Probability of orbital angular momentum for square Hermite-Gaussian vortex pulsed beam in oceanic turbulence channel[J]. Results in Physics, 2021, 28: 104590.

[13] Cao P F. Influence of anisotropic ocean turbulence on effective radius of curvature of partially coherent Hermite - Gaussian beam [J]. Canadian Journal of Physics, 2022, 100(3): 158-163.

[14] Tang M M, Zhao D M. Regions of spreading of Gaussian array beams propagating through oceanic turbulence[J]. Applied Optics, 2015, 54(11): 3407-3411.

[15] Lu L, Wang Z Q, Zhang J H, et al. Average intensity of $M\times N$ Gaussian array beams in oceanic turbulence[J]. Applied Optics, 2015, 54(25): 7500-7507.

[16] Yousefi M, Kashani F D, Mashal A. Analyzing the average intensity distribution and beam width evolution of phase-locked partially coherent radial flat-topped array laser beams in oceanic turbulence[J]. Laser Physics, 2017, 27(2): 026202.

[17] Mao Y H, Mei Z R, Gu J G, et al. Radial Gaussian-Schell-model array beams in oceanic turbulence[J]. Applied Physics B, 2017, 123(4): 111.

[18] 杨婷. 湍流对部分相干环状偏心光束和厄米-高斯光束传输特性的影响[D]. 成都: 四川师范大学, 2016.
Yang T. Influence of turbulence on propagation characteristics of partially coherent annular eccentric beams and Hermite-Gaussian beams[D].Chengdu: Sichuan Normal University, 2016.

[19] 陈晓文, 李宾中, 汤明玥. 部分相干厄米高斯光束的湍流距离[J]. 西华师范大学学报(自然科学版), 2014, 35(1): 82-86.
Chen X W, Li B Z, Tang M Y. Turbulence distance of partially coherent Hermite-Gaussian beams[J]. Journal of China West Normal University (Natural Sciences Edition), 2014, 35(1): 82-86.

[20] 汤明玥. 湍流对厄米高斯及列阵双曲余弦高斯光束的传输和远场光束质量的影响[D]. 成都: 四川师范大学, 2008.
Tang M Y. Influence of turbulence on propagation and far-field beam quality of Hermite Gaussian and array hyperbolic cosine Gaussian beams[D]. Chengdu: Sichuan Normal University, 2008.

[21] 张笔灵, 徐勇根, 王晓艳, 等. 厄米高斯相关谢尔模型光束在非 Kolmogorov 湍流的漂移[J]. 应用激光, 2018, 38(4): 630-636.
Zhang B L, Xu Y G, Wang X Y, et al. Beam wander of Hermite Gaussian correlated Schell-model beam in non-Kolmogorov turbulence[J]. Applied Laser, 2018, 38(4): 630-636.

[22] Yang T, Xu Y G, Tian H H, et al. Comparative study of propagation properties of partially coherent standard and elegant Hermite-Gaussian beams in inhomogeneous atmospheric turbulence[J]. Optik, 2016, 127(22): 10772-10779.

[23] Zhao J L, Wang G Q, Yin Y, et al. Propagation of a Hermite-cos-Gaussian correlated Schell-model beam in non-Kolmogorov turbulence[J]. Optik, 2021, 241: 167237-167245.

[24] Du X, Feng H, Du H, et al. Transmission characteristics of

linear Gaussian array beams propagating through seawater to air [J]. Optical Engineering, 2022, 61(11): 116101.
[25] Gbur G, Wolf E. Spreading of partially coherent beams in random media[J]. Journal of the Optical Society of America A, 2002, 19(8): 1592-1598.

Transmission Characteristics of Hermite-Gaussian Beam in Oceanic Turbulence

Du Xing[1,2], Ding Guixuan[1,2], Du Hao[1,3*], Wang Sheng[1,2], Feng Hui[1,3]

[1]*Aerospace Information Research Institute, Chinese Academy of Sciences, Beijing* 101408, *China*;
[2]*University of Chinese Academy of Sciences, Beijing* 100049, *China*;
[3]*Key Laboratory of Earth Observation of Hainan Province, Hainan Aerospace Information Research Institute, Wenchang* 571300, *Hainan*, *China*

Abstract

Objective In practical applications, communication between underwater platforms typically employs super low frequency/very low frequency (SLF/VLF) with narrow transmission bandwidths and insufficient security. Underwater laser communication has become a research hotspot due to its potential to provide higher transmission bandwidths and smaller transmission delay. However, adopting a Gaussian beam as a carrier of laser communication signals for underwater communication is limited by oceanic turbulence, which weakens the beam intensity and causes beam wander, beam expansion, and light intensity fluctuation to restrict the distance of underwater laser communication. To this end, we propose to utilize a Hermite-Gaussian beam for laser communication in oceanic turbulence. While this technique has been demonstrated in atmospheric turbulence, the mean square beam width, Rayleigh range, and turbulence distance in oceanic turbulence have not been reported. Therefore, our paper aims to build a beam transmission model in oceanic turbulence and analyze the mean square beam width, Rayleigh range, and turbulent distance. Finally, a more effective solution is provided for underwater laser communication technology, which can improve communication quality and extend the communication distance, thereby enabling more effective underwater exploration and resource development.

Methods The research methodology involves the study on propagation properties of partially coherent Hermite-Gaussian beams in oceanic turbulence. Our study begins by developing an intensity analysis model of Hermite-Gaussian beams in oceanic turbulence based on the extended Huygens-Fresnel principle. Then, the mean square beam width, Rayleigh range, and turbulent distance of Hermite-Gaussian beams in oceanic turbulence are derived. The expressions are obtained by the analytical approach based on the proposed intensity analysis model. Finally, the simulation analysis of the mean square beam width, Rayleigh range, and turbulent distance of Hermite-Gaussian beams in oceanic turbulence is conducted. The proposed theoretical model is adopted for analyzing the propagation of Hermite-Gaussian beams in seawater. The relationship between the parameters such as the Rayleigh range and the oceanic turbulence parameters is studied, and a reasonable physical interpretation is given. We provide a theoretical framework for analyzing the propagation properties of partially coherent Hermite-Gaussian beams in oceanic turbulence. The results can be leveraged to improve the performance of underwater laser communication systems.

Results and Discussions We investigate the effect of oceanic turbulence parameters on the mean square beam width, Rayleigh range, and turbulent distance of Hermite-Gaussian beams in oceanic turbulence. The results indicate that the mean square beam width increases with the rising mean square temperature dissipation rate. Additionally, the mean square beam width decreases with the dissipation rate of turbulent kinetic energy and decreases to a greater extent when the parameter w takes smaller values. Meanwhile, the larger parameter w determines the larger mean square beam width when salinity dominates. We also find that the mean square beam width increases with the transmission distance. The coherence length has less influence on the beam width and a larger coherence length results in a smaller beam width. The order of the Hermite-Gaussian beam also influences the beam width, and a higher order corresponds to a larger beam width. The Rayleigh range of the beam decreases with the mean square temperature dissipation rate and the relevant parameter w of temperature and salinity and increases with the turbulent kinetic energy dissipation rate. Finally, the turbulent distance decreases with the increase in the mean square temperature dissipation rate and the parameter w, and rises with the turbulent kinetic energy dissipation rate. Our findings have important implications for the design and

optimization of underwater optical communication systems.

Conclusions Our paper presents a study on the propagation properties of partially coherent Hermite-Gaussian beams in oceanic turbulence. We derive the expression for the cross spectral density function of the Hermite-Gaussian beam by the extended Huygens-Fresnel principle. We then investigate the effects of oceanic turbulence parameters and optical parameters on the Hermite-Gaussian beam transmission characteristics. The results show that the mean square beam width of the Hermite-Gaussian beam increases with the mean square temperature dissipation rate and the relative parameters of temperature and salinity, while it decreases with the dissipation rate of turbulent kinetic energy. In addition, the higher order Hermite-Gaussian beam means a larger mean square beam width, and both the Rayleigh range and the turbulent distance increase with the rising beam order. These findings suggest that higher-order Hermite-Gaussian beams are more resistant to turbulent perturbations and can lead to longer effective communication distances. Our study is significant for underwater laser communication research and provides insight into the optimal design parameters for communication systems operating in oceanic turbulence.

Key words underwater optical communication; Hermite-Gaussian beam; oceanic turbulence; transmission characteristics